



# CHORUS

This is the accepted manuscript made available via CHORUS. The article has been published as:

## Flow in a containerless liquid system: Ring-sheared drop with finite surface shear viscosity

Shreyash Gulati, Frank P. Riley, Amir H. Hirska, and Juan M. Lopez

Phys. Rev. Fluids **4**, 044006 — Published 16 April 2019

DOI: [10.1103/PhysRevFluids.4.044006](https://doi.org/10.1103/PhysRevFluids.4.044006)

# Flow in a containerless liquid system: Ring-sheared drop with finite surface shear viscosity

Shreyash Gulati, Frank P. Riley, and Amir H. Hirs  
*Rensselaer Polytechnic Institute, Troy, New York, USA*

Juan M. Lopez\*  
*Arizona State University, Tempe, Arizona, USA*

(Dated: April 4, 2019)

## Abstract

The ring-sheared drop is a new flow configuration for microgravity, where surface tension provides containment and shear in the bulk is driven primarily by the action of surface shear viscosity. A drop is constrained by two thin contact rings, one stationary at a southern latitude and the other at the same latitude but in the north and rotating. Since we consider a microgravity setting, the drop is not restricted to being small. Furthermore, we allow for arbitrarily small surface shear viscosity, so that in general the interfacial and bulk flows are viscously coupled. Our numerical simulations show that even small surface shear viscosity (quantified nondimensionally by a Boussinesq number) can produce a significant meridional bulk flow at moderate ring rotation rates (quantified by a Reynolds number  $Re$ ). At very low  $Re$ , the bulk flow is viscously dominated and surface viscosity makes very little difference. At high  $Re$ , the secondary flow is very weak if the surface viscosity is negligible and the flow tends toward solid-body rotation.

---

\* [jmlopez@asu.edu](mailto:jmlopez@asu.edu)

## I. INTRODUCTION

A microgravity environment offers unique capabilities for studying hydrodynamics, including the possibility of surface tension-containment at the macroscale. Even with a large  $g$ -jitter and considering  $10^{-3} g_0$  instead of microgravity ( $10^{-6} g_0$ ), the capillary length  $\sqrt{\sigma/\rho g}$  is over 8 cm for aqueous systems, where  $\sigma$  is the surface tension,  $\rho$  is the density,  $g$  is the local acceleration, and  $g_0$  is Earth's gravitational acceleration. Consequently, flow experiments are feasible for a drop of water that is hundreds of cubic centimeters in volume. Surface tension containment is especially useful in liquid systems where contact with solid walls can affect the liquid through chemical, sorption, or electrostatic interactions. Also, in biological systems there may be some advantages in using aqueous systems without solid walls, in part because biofilm formation is fundamentally different at solid boundaries as compared to free surfaces. This has significant consequences for microorganisms and their evolution at the air-water interface [1].

The ring-sheared drop is an experiment for the International Space Station to study shearing flow in the absence of solid walls. The module is designed to shear a 2.54 cm diameter drop of water with dissolved protein. The drop is constrained by a pair of circular contact rings, one at a northern latitude and the other in the same latitude in the south, as depicted in Fig. 1. The ring size and the distance between them is such that when static, the drop is exactly spherical. In the ring-sheared drop, one of the contact rings is steadily rotated while the other is stationary. Shearing flow is conveyed into the drop primarily by the action of surface shear viscosity. In the presence of macromolecules such as proteins at the interface as well as in most biological systems, it is expected that the surface shear viscosity is large enough so that significant shear flow is driven in the bulk by the rotation of a ring. The ring-sheared drop experiment is currently focused on studying the biophysics of protein amyloid fibrils, the waxy plaque which destroys the neurons of people with Alzheimers disease [2]. Hydrodynamic stresses appear to play a major role in the transport and accumulation of pre-fibrils in the brain [3]. Shear stress has been shown to significantly accelerate amyloidogenesis in a Couette apparatus [4].

The flow in the ring-sheared drop was examined recently for its mixing characteristics [5]. In that study, the Boussinesq number  $Bo$ , which is the ratio of the surface shear viscosity to the product of the viscosity in the bulk and the length scale, was taken to be  $Bo \rightarrow \infty$ . In that limit, the interfacial flow decouples from the bulk flow and the azimuthal velocity at the interface can be obtained analytically, providing the boundary condition for bulk flow simulations [5]. Here, we relax the assumption of  $Bo \rightarrow \infty$  to study the flow field in large drops as well as in liquid systems with arbitrarily small surface shear viscosity.

## II. GOVERNING EQUATIONS AND NUMERICAL TECHNIQUE

Consider a liquid drop of radius  $R$ , in a zero gravity environment, constrained by two rings, each of radius  $A$ , at polar angles  $\theta = 45^\circ$  and  $\theta = 135^\circ$ , as depicted in Fig. 1(a). The

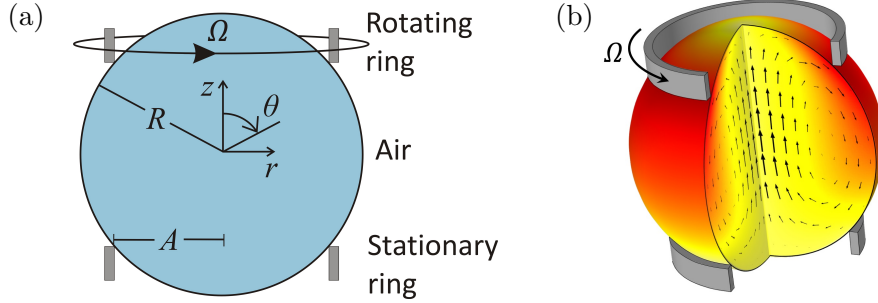


FIG. 1. (a) Schematic of the ring-sheared drop and (b) a three-dimensional view of the flow in the limit of a large surface shear viscosity. Colors in the panel (b) represent the azimuthal velocity ranging from yellow (minimum) to red (maximum). The vectors in the panel (b) show the secondary flow in the  $(r, z)$ -meridional plane.

top (northern) ring rotates with an angular velocity  $\Omega$  and the bottom (southern) ring is stationary.

The flow is solved using cylindrical coordinates  $(r, \phi, z)$ , and corresponding velocity  $\mathbf{u} = (u, v, w)$ . The flow in the drop is governed by the Navier–Stokes equations, which are non-dimensionalized with length scale  $R$  and time scale  $1/\Omega$ :

$$\partial_t \mathbf{u} + (\mathbf{u} \cdot \nabla) \mathbf{u} = -\nabla p + \frac{1}{\text{Re}} \nabla^2 \mathbf{u}, \quad \nabla \cdot \mathbf{u} = 0, \quad (1)$$

where  $\text{Re} = \Omega R^2/\nu$  is the Reynolds number, giving the ratio of viscous time  $R^2/\nu$  to rotation time  $1/\Omega$ , and  $\nu$  is the kinematic viscosity of the bulk.

Throughout this study we take the ratio of ring to drop radii  $A/R = 1/\sqrt{2}$ , and assume that the drop remains spherical so that the drop interface is at  $(r, \phi, z) = (R \sin \theta, \phi, R \cos \theta)$ , with  $\theta \in [0, \pi]$  and  $\phi \in [0, 2\pi)$ . Also, we assume the flow remains axisymmetric (i.e.  $\partial_\phi = 0$ ); this will be true for  $\text{Re}$  not too large. The rotating ring is at polar angle  $\theta = 45^\circ$ , corresponding to  $(r, z) = (1/\sqrt{2}, 1/\sqrt{2})$  and the stationary ring is at polar angle  $\theta = 135^\circ$ , corresponding to  $(r, z) = (1/\sqrt{2}, -1/\sqrt{2})$ . The no-slip boundary conditions at the rings are  $\mathbf{u}(1/\sqrt{2}, \phi, 1/\sqrt{2}) = (0, 1/\sqrt{2}, 0)$  and  $\mathbf{u}(1/\sqrt{2}, \phi, -1/\sqrt{2}) = (0, 0, 0)$ . Symmetry dictates that  $u = 0$ ,  $v = 0$  and  $\partial_r w = 0$  along the axis ( $r = 0$ ). That leaves the interfacial condition to be dealt with.

The interface is assumed to be Newtonian and governed by the Boussinesq–Scriven surface model [6–8], with surface-excess pressure tensor

$$\mathbf{T}^s = \sigma \mathbf{I}_s + \boldsymbol{\tau}^s, \quad (2)$$

where  $\boldsymbol{\tau}^s$  is the surface-excess stress tensor

$$\boldsymbol{\tau}^s = [(\kappa^s - \mu^s) \nabla_s \cdot \mathbf{u}^s] \mathbf{I}_s + 2\mu^s \mathbf{D}^s, \quad (3)$$

$\sigma$  is the surface tension,  $\mu^s$  is the surface shear viscosity,  $\kappa^s$  is the surface dilatational viscosity,  $\nabla_s$  is the surface gradient operator,  $\mathbf{u}^s = (u^s, v^s, w^s)$  is the surface velocity vector,

$\mathbf{I}_s$  is the surface projection tensor and  $\mathbf{D}^s$  is the surface rate of deformation tensor, such that

$$2\mathbf{D}^s = \nabla_s \mathbf{u}^s \cdot \mathbf{I}_s + \mathbf{I}_s \cdot (\nabla_s \mathbf{u}^s)^T. \quad (4)$$

Taking the surface gradient of (2) gives

$$\nabla_s \cdot \mathbf{T}^s = \nabla_s \sigma + \nabla_s [(\kappa^s - \mu^s) \nabla_s \cdot \mathbf{u}^s] + [\sigma + (\kappa^s - \mu^s) \nabla_s \cdot \mathbf{u}^s] \nabla_s \cdot \mathbf{I}_s + 2(\nabla_s \mu^s) \cdot \mathbf{D}^s + 2\mu^s \nabla_s \cdot \mathbf{D}^s. \quad (5)$$

Assuming a non-deforming interface, i.e. the drop remains spherical, the normal component of velocity at the interface is identically zero. Furthermore, for aqueous systems driven with modest ring speeds, the capillary number  $\mu\Omega R/\sigma$  will be small, where  $\mu$  is the dynamic viscosity of the bulk liquid. We have previously shown through experiments and computations that for a system with small capillary number, a minuscule surface tension gradient is sufficient to stop what would be a polar velocity at the drop interface [9, 10]. Thus, the surface stress balance in the surface normal and polar tangential directions reduces to  $u^s = w^s = 0$ .

Since the only non-zero component of the surface velocity vector is the azimuthal component  $v^s$ , there are no surface dilatational effects. Furthermore, since only a small gradient in surface concentration is sufficient to arrest the polar flow at the interface, the surface shear viscosity will have negligible gradients. Then, (5) reduces to

$$\nabla_s \cdot \mathbf{T}^s = 2\mu^s \nabla_s \cdot \mathbf{D}^s, \quad (6)$$

and the interfacial stress balance in the azimuthal direction can be written as

$$(f_1 \partial_{rr} + f_2 \partial_{zz} + f_3 \partial_{rz} + f_4 \partial_r + f_5 \partial_z + f_6) v = \frac{1}{\text{Bo}} (r \partial_r + z \partial_z - 1) v, \quad (7)$$

where  $\text{Bo} = \mu^s/(\mu R)$  is the Boussinesq number and the non-constant coefficients are  $f_1 = 1 - 2r^2 + r^2 z^2 + r^4$ ,  $f_2 = 1 - 2z^2 + r^2 z^2 + z^4$ ,  $f_3 = -2rz$ ,  $f_4 = 1/r - 3r + rz^2 + r^3$ ,  $f_5 = -3z + r^2 z + z^3$ ,  $f_6 = 2 - 1/r^2$ . All the terms in (7) are evaluated at the interface, and the solution is the azimuthal velocity at the interface,  $v^s$ . Equation (7) provides the viscous coupling between the interfacial and bulk flows. The right-hand-side of (7) is the viscous stress exerted by the bulk and the left-hand side is the surface viscous stress.

The range of flow parameters considered in this study are meant to cover the values anticipated in the ISS experiments. The maximum ring rotation rate, and hence the maximum Reynolds number, is limited by inertia affecting the drop shape. Thus the Weber number, which is the ratio of inertial forces to surface tension forces, sets the maximum rotation rate and in turn the maximum Re. Following [5], and using a conservative value of 0.1 for the Weber number, the corresponding ring rotation rate  $\Omega$  is found to be about 30 revolutions per minute, and the corresponding Reynolds number is  $\text{Re} \approx 500$ . In the present numerical study, we consider  $\text{Re} \in [1, 1000]$ . The range of Boussinesq numbers Bo expected for the ISS experiment range from a minimum of about 0.05 to over 100, based on the surface shear viscosity measurements of insulin reported in [10]. Presently, we consider  $\text{Bo} \in [10^{-4}, 100]$ .

The numerical method employed for solving the flow inside the drop is similar to that in [5], using COMSOL’s FEM-based modeling. The coupling between the bulk flow and the interfacial flow is accomplished by evaluating the azimuthal velocity gradients from the bulk flow at the interface to get the right-hand side of (7). Then, the surface azimuthal component of velocity, obtained by solving (7), is used as the surface boundary condition in solving for the bulk flow. Second-order shape functions were used for velocity. A boundary-layer mesh in the bulk was constructed near the interface, with a fine distribution of nodes near the interface. The bulk mesh consisted of 53 731 quadrilateral elements, with a base mesh-element size of 0.02, and the finest size being approximately  $2 \times 10^{-4}$ . A transient solver with adaptive time-stepping was utilized for nine cases with  $\text{Bo} = 100, 1$  and  $10^{-4}$  and  $\text{Re} = 10, 100$  and  $1000$ . In all these cases, the flows evolved to steady state. A steady-state solver was also used to simulate these cases and the results were in very close agreement with transient results. Therefore, in order to reduce compute times, the steady-state solver was used for all other cases.

### III. RESULTS

We begin by examining the large Boussinesq number limit, corresponding to a highly viscous interface. In the limit  $\text{Bo} \rightarrow \infty$ , the right-hand side of (7) vanishes and the equation can be solved analytically for the azimuthal velocity at the interface [5]:

$$v^s = \begin{cases} \sin \theta, & \text{for } \theta \in [0^\circ, 45^\circ), \\ 0.5 \sin \theta + 0.308 [\cot \theta - \sin \theta \ln (\csc \theta - \cot \theta)] / \sqrt{2}, & \text{for } \theta \in [45^\circ, 135^\circ], \\ 0, & \text{for } \theta \in (135^\circ, 180^\circ]. \end{cases} \quad (8)$$

In the region north of the rotating ring,  $\theta \in [0^\circ, 45^\circ)$ , the flow at the interface is in solid-body rotation with surface azimuthal velocity  $v^s = r = \sin \theta$ , so it acts as a (no-slip) rotating endcap. Similarly, in the region south of the stationary ring,  $\theta \in [135^\circ, 180^\circ)$ , the interface is stagnant and behaves as a stationary endcap. In between the two rings, the interface is sheared azimuthally. The situation is analogous to a rotor-stator, which has been extensively studied when the rotor and stator are flat disks. In the limit of  $\text{Bo} \rightarrow \infty$ , the interfacial flow is completely decoupled from the bulk flow, but of course the flow in the bulk is driven by the interfacial flow and depends on the Reynolds number.

For all Reynolds numbers considered ( $\text{Re} \in [1, 1000]$ ), using Boussinesq numbers  $\text{Bo} \gtrsim 10^2$  results in an interfacial velocity profile that is indistinguishable from the  $\text{Bo} \rightarrow \infty$  analytic solution (8). Figure 2 compares the analytic profile to that at  $\text{Bo} = 100$  for both  $\text{Re} = 10$  and  $1000$ ; the results are indistinguishable at the scale of the figure. However, for smaller  $\text{Bo}$ , the interfacial profile is very much  $\text{Re}$  dependent. Figure 3 summarizes how the interfacial profile varies with  $\text{Bo}$  and  $\text{Re}$ .

Figure 3(a) shows the interfacial velocity profiles for  $\text{Re} = 10$  and a wide range of  $\text{Bo}$ . At this low  $\text{Re}$ , the velocity profile for  $\text{Bo} = 1$  is very similar to that at  $\text{Bo} = 100$ , indicating the interfacial flow remains essentially decoupled from the bulk flow. However, for much smaller

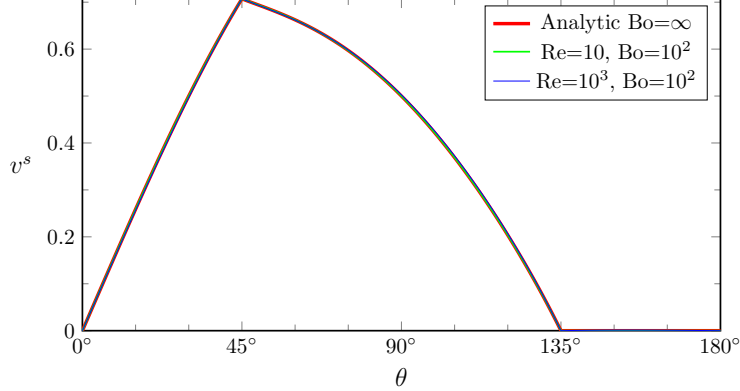


FIG. 2. Numerical profiles of surface azimuthal velocity  $v^s$  at  $\text{Re} = 10$  and  $\text{Re} = 1000$ , both with  $\text{Bo} = 100$  compared to the analytic profile from (8).

$\text{Bo} = 10^{-2}$  there is sufficient viscous coupling between the bulk and the interface so that the right-hand side of (7), the viscous stress exerted by the bulk, is no longer negligible. Now, the strength of the coupling is not only determined by  $\text{Bo}$  but also by  $\text{Re}$ . Figures 3(b) and (c) show the interfacial profiles for  $\text{Re} = 100$  and  $1000$  for the same  $\text{Bo}$  as in (a). For  $\text{Bo} = 1$  there are gradual departures from the analytic profile at  $\text{Bo} \rightarrow \infty$  with increasing  $\text{Re}$ . For  $\text{Bo} \rightarrow 0$  all the profiles approach  $v^s = 0.5 \sin \theta$  with the larger  $\text{Re}$  cases approaching this faster as  $\text{Bo}$  is reduced, except at  $\theta = 45^\circ$  and  $135^\circ$  where the rotating and stationary rings are located. The profile  $v^s = 0.5 \sin \theta$  corresponds to solid-body rotation at the average rotation rate of the two rings. The departure from this in the case  $\text{Re} = 100$  and  $\text{Bo} = 10^{-4}$  is localized to within a few degrees from the two rings.

We now consider the structure of the corresponding bulk flow. The first column of Fig. 4 shows the vortex lines (contours of  $\gamma = rv$ ) and the azimuthal vorticity ( $\eta = \partial_z u - \partial_r w$ ) for  $\text{Bo} = 100$  and  $\text{Re} = 10, 100$  and  $1000$ . As we saw in Fig. 3, in this parameter regime the interface is decoupled, and the interfacial profile is essentially that at  $\text{Bo} \rightarrow \infty$ . The bulk flow that is driven by this profile however, depends on  $\text{Re}$ . The northern endcap (the interface at  $0^\circ \leq \theta \leq 45^\circ$ ) acts like a rotating solid cap, the southern endcap (the interface at  $135^\circ \leq \theta \leq 180^\circ$ ) acts like a stationary cap, and the interface in between has no simple analogy as it is a non-uniformly sheared fluid interface. For all  $\text{Re}$  at this  $\text{Bo}$ , all the vortex lines enter the bulk from rotating northern endcap and terminate on the interface between the two ring; they cannot terminate on the stationary southern endcap. This means that the vortex lines are bent with respect to the rotation axis, driving a secondary meridional flow. For low  $\text{Re}$ , this meridional flow is weak, as quantified by the azimuthal vorticity. For axisymmetric flow, the vorticity  $\nabla \times \mathbf{u} = (-1/r \partial_z \gamma, \eta, 1/r \partial_r \gamma)$ . Surfaces of constant  $\gamma$  are axisymmetric vortex tubes; the vorticity vector at any point is tangent to the tube at that point [11]. The governing equation for  $\eta$  is readily obtained from the azimuthal component of the curl of the Navier–Stokes equations:

$$(\partial_t + u\partial_r + w\partial_z - u/r) \eta - \frac{2\gamma}{r^3} \partial_z \gamma = \frac{1}{\text{Re}} \left( \partial_{zz} + \partial_{rr} + \frac{1}{r} \partial_r - \frac{1}{r^2} \right) \eta. \quad (9)$$

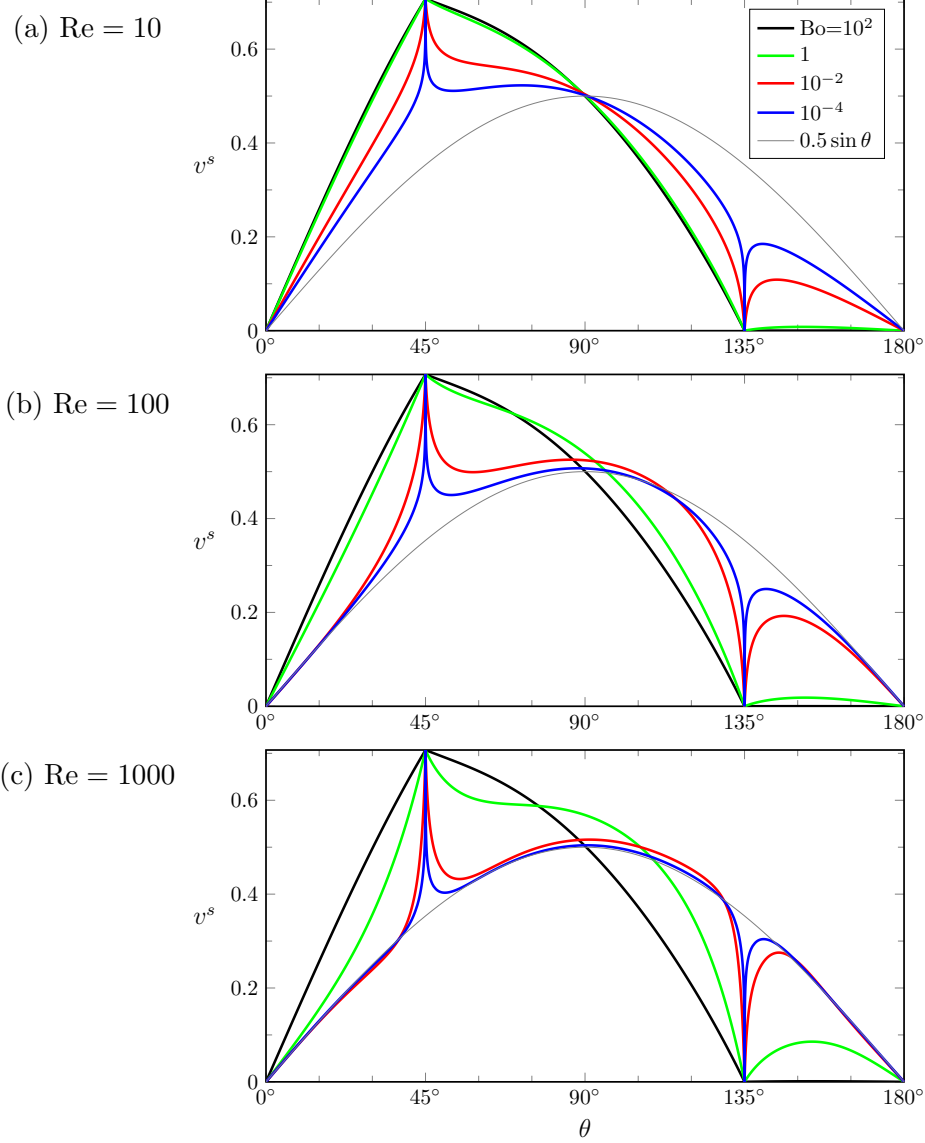


FIG. 3. Profiles of the surface azimuthal velocity  $v^s$  for Re and Bo as indicated.

If the vortex tubes are not right-circular cylinders, then  $\partial_z \gamma \neq 0$  and this appears in the last term on the left-hand side of (9), driving the meridional flow. For increasing Re, the meridional flow is stronger and is able to advect the vortex lines with it. By Re = 1000 there is an Ekman-like boundary layer on the rotating northern endcap and a Bödewadt-like boundary layer on the stationary southern endcap, and the bulk flow in between is rotating as a solid-body at approximately the average rate of the two rings. General properties of Ekman and Bödewadt boundary layers are described, for example in Schlichting and Gersten [12]. As Bo is decreased, the southern interface is no longer a stationary endcap and the vortex lines can now terminate there. At the largest Re and smallest Bo in the figure, the vortex lines are parallel to the rotation axis, except very near the two rings, matching the solid-body rotation at the average rate of the two rings described earlier for

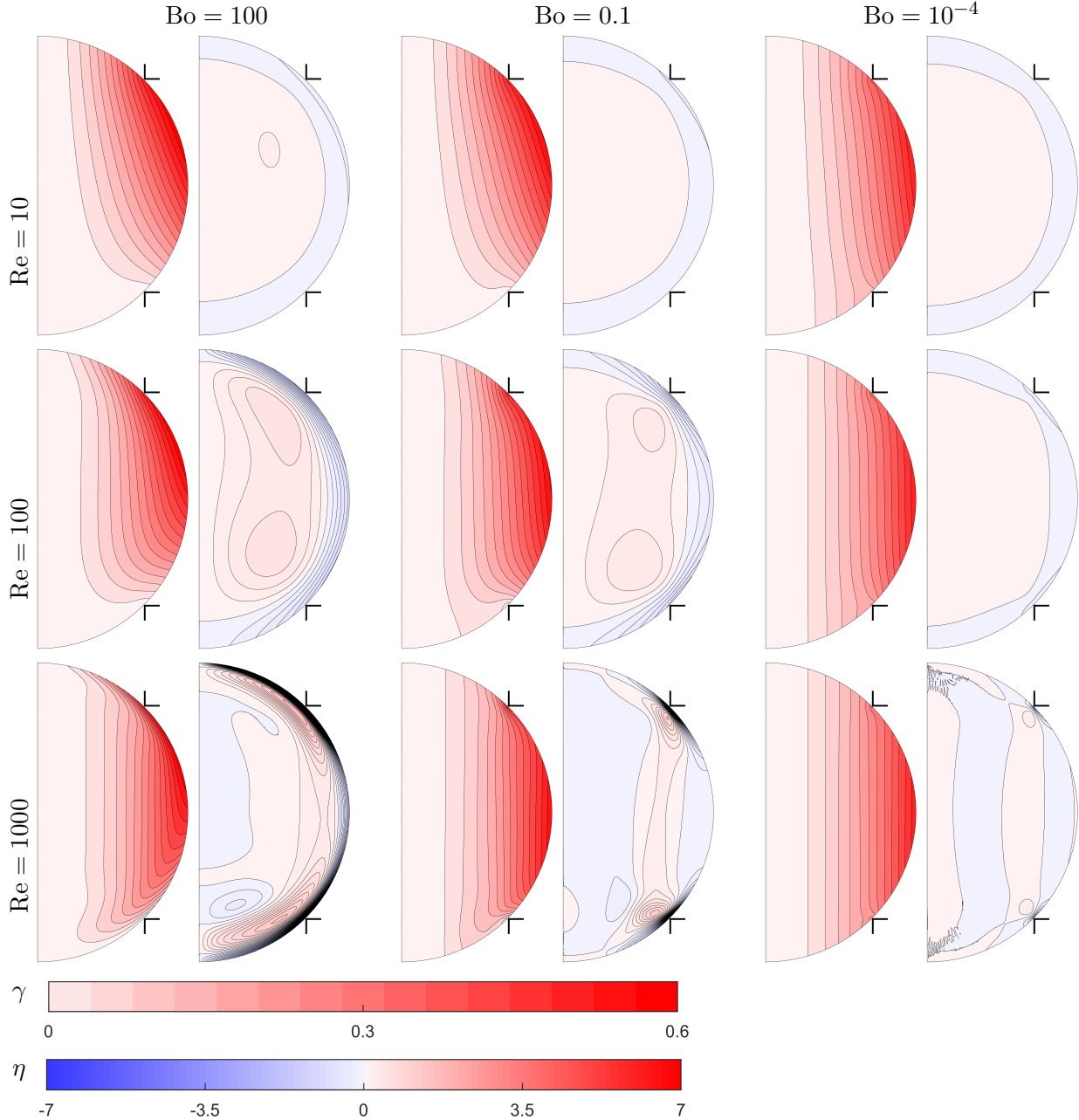


FIG. 4. Contours of vortex lines  $\gamma$  (left) and azimuthal vorticity  $\eta$  (right), for Re and Bo as indicated. There are 15 levels in  $\gamma \in [0, 0.6]$  and 50 levels in  $\eta \in [-7, 7]$ .

the interfacial velocity. Now that there is essentially no vortex line bending, the meridional flow has vanished (except very local to the rings).

We now consider the energetics of the flow, specifically, the viscous dissipation in the bulk. The volume integral of the (nondimensional) viscous dissipation rate is

$$\Phi = \frac{1}{V} \int_V [2(\partial_r u)^2 + 2u^2/r^2 + 2(\partial_z w)^2 + (r\partial_r(v/r))^2 + (\partial_z u + \partial_r w)^2 + (\partial_z v)^2] dV, \quad (10)$$

where  $V = 4\pi/3$  is the (nondimensional) volume of the drop. Note that the dimensional

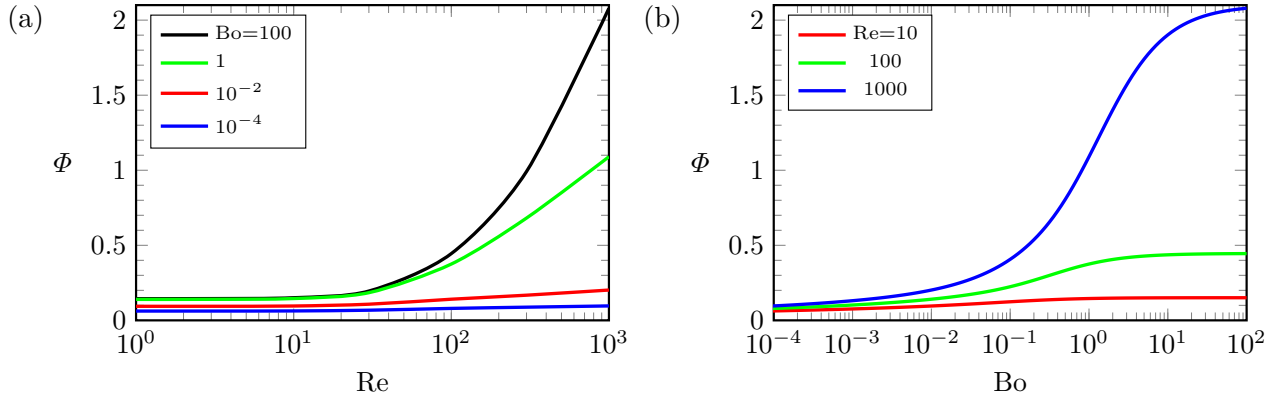


FIG. 5. Variation of the viscous dissipation rate  $\Phi$  with Bo and Re as indicated.

viscous dissipation is obtained by multiplying by  $\mu\Omega^2$ . Figure 5 shows  $\Phi$  as a function of Bo and Re. For a given drop size and viscosity in the bulk, each Re corresponds to some angular velocity of the ring. Figure 5(a) shows that the nondimensional viscous dissipation does not vary with Re when the bulk flow is in the viscous-dominated regime, i.e. for  $Re \lesssim 25$ . In this regime, there is a very weak dependence on Bo with  $\Phi$  slowly increasing with Bo until  $Bo \sim 1$ , beyond which it becomes independent of Bo as well. For  $Re > 25$ , bulk inertia effects become important, and the dependence for larger  $Re$  is of the form  $\Phi \propto c_r \log Re$ , where the rate ‘constant’  $c_r$  increases with  $Bo$ . This increase in the dissipation is due to the development of an intense boundary layer at the drop interface (see Fig. 4). This is in contrast to the small Bo cases where the dissipation is solely localized to where the rings contact the drop. Figure 5(b) shows that  $\Phi$  begins to increase rapidly for  $Bo \gtrsim 10^{-1}$  and saturates at larger values of Bo with increasing Re.

#### IV. DISCUSSION AND CONCLUSIONS

The ring-sheared drop is a novel flow system for use in microgravity, where surface tension provides containment and the mixing in the bulk is primarily driven by the action of surface shear viscosity. The drop is constrained by a stationary ring at a southern latitude and sheared by constant rotation of a ring at a northern latitude. An earlier study focused on the mixing in this system for a sufficiently small drop such that the surface shear viscosity dominates over the viscosity in the bulk, leading to the Boussinesq number  $Bo \rightarrow \infty$ , where the interfacial hydrodynamics is decoupled from the bulk flow. Here, we have relaxed this assumption and find that for  $Bo \gtrsim 100$  the interfacial flow is also essentially decoupled from the bulk. This is consistent with what happens in a knife-edge viscometer, in which fluid in a stationary cylindrical container is sheared by a rotating contact ring at the flat free surface [13]. For  $Re \lesssim 10$ , there is very little response to variations in Bo. In the other limit,  $Bo \rightarrow 0$ , the bulk is spun up to solid-body rotation at half the rotation rate of the ring (i.e. average rotation of the two rings), except near the rings due to the spike in azimuthal velocity and the corresponding secondary flow. In contrast, in the knife-edge viscometer

there is very little bulk flow due to the viscous dissipation at the walls of the stationary solid container. In between the limits of large and small  $Bo$ , both the interfacial and bulk flows smoothly transition between the two limit flows. Large  $Bo$  results in a flow that is very reminiscent of a rotor-stator, with an Ekman layer on the endcap between the north pole and the rotating ring and a Bödewadt layer on the endcap between the south pole and the stationary ring. The interfacial velocity was found to be insensitive to  $Bo$  near the equator, unless  $Re$  is very large and/or  $Bo$  is very small, and of course at the poles due to axisymmetry for all  $Re$  and the rings due to no-slip there. Furthermore, if the ring-sheared drop is to be used as a bioreactor in microgravity, the relevant  $Bo$  is of order 1 (since the drop size is large and the surface viscosity is modest), the results show that  $Re \sim 100$  provides good mixing (vortex lines are bent and the flow is far from solid-body rotation) and at the same time the boundary layers near the rings are not very intense and so any damage to microorganisms from the associated shear stresses is expected to be minimal.

## ACKNOWLEDGMENTS

This work was supported by NASA grant NNX13AQ22G.

- 
- [1] P. B. Rainey and M. Travisano, “Adaptive radiation in a heterogeneous environment,” *Nature* **394**, 69–72 (1998).
  - [2] C. Dobson, “Protein misfolding, evolution and disease,” *Trends Biochem. Sci.* **24**, 329–332 (1999).
  - [3] M. Nedergaard, “Garbage truck of the brain,” *Science* **340**, 1529–1530 (2013).
  - [4] S. A. McBride, S. P. Sanford, J. M. Lopez, and A. H. Hirs, “Shear-induced amyloid fibrilization: role of inertia,” *Soft Matter* **12**, 3461–3467 (2016).
  - [5] S. Gulati, F. P. Riley, J. M. Lopez, and A. H. Hirs, “Mixing within drops via surface shear viscosity,” *Intl. J. Heat Mass Transf.* **125**, 559–568 (2018).
  - [6] L. E. Scriven, “Dynamics of a fluid interface. Equation of motion for Newtonian surface fluids,” *Chem. Eng. Sci.* **12**, 98–108 (1960).
  - [7] D. A. Edwards, H. Brenner, and D. T. Wasan, *Interfacial Transport Processes and Rheology* (Butterworth–Heinemann, Boston, 1991).
  - [8] J. C. Slattery, L. Sagis, and E.-S. Oh, *Interfacial Transport Phenomena*, 2nd ed. (Springer: New York, 2007).
  - [9] A. H. Hirs, J. M. Lopez, and R. Miraghaie, “Determination of surface shear viscosity via deep-channel flow with inertia,” *J. Fluid Mech.* **470**, 135–149 (2002).
  - [10] V. S. Balaraj, P. C. Zeng, S. P. Sanford, S. A. McBride, A. Raghunandan, J. M. Lopez, and A. H. Hirs, “Surface shear viscosity as a macroscopic probe of amyloid fibril formation at a fluid interface,” *Soft Matter* **13**, 1780–1787 (2017).
  - [11] J. M. Lopez and A. D. Perry, “Axisymmetric vortex breakdown: Part 3. Onset of periodic flow and chaotic advection,” *J. Fluid Mech.* **234**, 449–471 (1992).

- [12] H. Schlichting and K. Gersten, *Boundary-Layer Theory*, 9th ed. (Springer, 2017).
- [13] J. M. Lopez and A. H. Hirs, “Coupling of the interfacial and bulk flow in knife-edge viscometers,” *Phys. Fluids* **27**, 042102 (2015).